Available online at www.sciencedirect.com
ScienceDirect
Journal of Nuclear Materials 366 (2007) 306–316
journal of nuclear materials
www.elsevier.com/locate/jnucmat

Effect of sintering conditions on the microstructure and mechanical properties of ZrN as a surrogate for actinide nitride fuels

K. Wheeler [a,b,*], P. Peralta [a], M. Parra [a], K. McClellan [b], J. Dunwoody [c], G. Egeland [b]

[a] Mechanical and Aerospace Engineering, Arizona State University, P.O. Box 876106, Tempe, AZ 85287, USA
[b] Material Science and Technology Division, Los Alamos National Laboratory, Los Alamos, NM 87545, USA
[c] Nuclear Materials Technology Division, Los Alamos National Laboratory, Los Alamos, NM 87545, USA

Abstract

Pellets of sintered ZrN were studied to optimize the mechanical properties and microstructures needed in nitride fuel pellets, using ZrN as a surrogate for actinide nitrides and as potential component in low fertile and inert matrix fuels. Samples were prepared via sintering in either Ar or N_2 (with and without 6% H_2) and at 1300 °C or 1600 °C. A significant difference in the hardness was measured ranging from 1000 (Kg/mm^2) in samples sintered at 1600 °C in argon to 100 (Kg/mm^2) in samples sintered at 1300 °C in nitrogen. Samples with 6% hydrogen added to the sintering environment experienced a decrease in hardness, as well as an increase in intergranular cracking as compared to samples sintered without hydrogen, suggesting hydrogen embrittlement. Grain size was more uniform in samples sintered in pure Ar as compared to Ar–H_2, while the latter had a larger fraction of high angle grain boundaries than the former. Cracking around indents had a clear tendency to follow high angle boundaries, which were found to be intrinsically weak in ZrN.
Published by Elsevier B.V.

PACS: 81.05.Je; 89.30.Gg; 62.20.Qp; 81.20.Ev

1. Introduction

Nuclear fuels based on actinide nitrides, particularly uranium and plutonium mononitrides and their solid solutions, have considerable potential for advanced applications, including nuclear power sources and nuclear–thermal propulsion for space vehicles [1–4]. Research carried out so far indicates that nitride fuels have a series of quite desirable properties, including high thermal conductivity, high melting point, high actinide atomic density, low swelling and low fission gas release, among others [2,3,5]. Interest on nitride based fuels for advanced applications has arisen within the advanced fuel cycle initiative (AFCI) of the US Department of Energy (DOE), since these materials

* Corresponding author. Address: Material Science and Technology Division, Los Alamos National Laboratory, Los Alamos, NM 87545, USA. Tel.: +1 505 665 4043.
E-mail address: kirkwheeler@lanl.gov (K. Wheeler).

0022-3115/$ - see front matter Published by Elsevier B.V.
doi:10.1016/j.jnucmat.2007.03.023

are potential candidates for the development of fuels that could potentially enhance proliferation resistance of next generation of nuclear reactors, and for waste reduction via transmutation of transuranic fission products [6], thus reducing the environmental impact of nuclear energy production by reducing the long-lived radiation sources by a factor of 10 and radiotoxicity by a factor of 100 [1].

Due to the high cost associated with the development, testing and characterization of transuranic fuels, ZrN has been proposed as a surrogate material based on the fact that it is isostructural with many actinide mononitrides (NaCl structure), its ability to form a solid solution with PuN [7], the similarities observed between its microstructure and that of actinide nitrides [7], as well as being a possible inert matrix material to host minor actinide (MA: Np, Am, Cm) materials during transmutation [8–11].

The addition of the transuranics complicates the structural requirements of sintered fuel pellets for a few reasons. The fact that Am has a tendency to vaporize under typical sintering conditions [12,13] has called for the development of alternative sintering parameters to reduce Am losses. Furthermore, ^{241}Am can produce a large quantity of helium during irradiation from α-decay [14]. This extra gas could increase pellet swelling [15], cracking and accelerate the degradation of the mechanical integrity of the fuel. One possible approach for the controlled release of this extra gas requires the fuel pellet to have an increased percentage of open porosity while maintaining a high level of hardness and fracture toughness.

In order to optimize the mechanical properties and porosity distributions needed in sintered nitride fuel pellets, test samples of ZrN were prepared using a variety of sintering conditions. Relationships between the resulting microstructure, processing and mechanical properties were established and correlated with potential fuel performance. These correlations, along with the methodologies used, which include modern methodologies such as OIM that have not been extensively used to characterize nuclear fuels, can be useful in the development of nitride fuels for space reactors and other advanced applications.

2. Experimental procedure

The sintered ZrN pellets used for this study were prepared at Los Alamos National Laboratory (LANL) under various atmospheres and sintering temperatures. All of the pellets were made from the same batch of commercial –325 mesh ZrN powder, mixed with a lube and binder (0.2 wt% Zn Stearate and 0.3 wt% PEG) in a nitrogen gas filled glove box with <10 ppm O_2. Batches of 5 g of this mixture were milled in a Spex mill for 45 min and then pressed at 250 MPa. These pellets were then sintered at either 1600 °C or 1300 °C for 10 h plus thermal ramp time. Four different atmospheres were used for this study, UHP–Ar, Ar–6% H_2, UHP–N_2 and N_2–6% H_2. Pure ZrN powder was also poured over the pressed green pellets so that the powder could act as a sacrificial oxidation target thus reducing oxygen contamination. Note that the study performed by Matthews et al. [3] on UN for space fuels used sintering to produce fuel pellets, but only under pure gettered Ar, so a comparison can be established with the other sintering environments used here.

Metallographic samples were taken from the pellet's radial plane and polished using a 6 μm diamond impregnated disk, SiC paper (600, 800, and 1200 grit) and then finished with 0.05 μm colloidal silica. These metallographic samples were also used to measure Vickers hardness using a load of 500 g, which was found to be large enough to average out microstructural variations such as porosity and grain formations.

Fifteen indents per sample were made and optical microscopy was used to measure their diagonals for hardness calculation.

A small portion of the sintered samples were ground in an agate mortar along with high purity Si to perform standard X-ray powder diffraction using a Rigaku D/Max-IIB diffractometer with Cu Kα radiation. Intensity data were taken every 0.02° scanning at a rate of 2°/min. The Si served as an internal reference to correct for possible angular misalignments. The resulting diffraction patterns were indexed using standard databases and commercial software. Lattice parameters were determined by using a least squares fitting of the ZrN peaks assuming a NaCl structure.

The microstructure of the samples was characterized using scanning electron microscopy (SEM) and orientation imaging microscopy (OIM). SEM was performed in an FEI XL-30 environmental scanning electron microscope operating at 20 kV. Additional SEM and OIM imaging were performed on a Camscan scanning electron microscope with an EDAX/TSL OIM system.

A pellet of ZrN was prepared via Hot Isostatic Pressing (HIP) and was heat-treated for 36 h at 1400 °C in an N_2–6% H_2 environment. The sample was covered in pure ZrN powder during this heat treatment to reduce sample oxidation. Transmission Electron Microscopy (TEM) was performed on sections of this sample, before and after heat-treatment using a Philips/FEI CM-30 using a 300 keV beam.

3. Results and discussion

3.1. Physical characteristics

The sintered density and the open and closed porosities of the samples are shown in Fig. 1. It can be seen that the sintered density of the material is a strong function of temperature and sintering gas (Ar or N_2), but it does not depend strongly on the presence of hydrogen in the gas stream, and there is just a slight trend for lower density in the presence of hydrogen. The effect of sintering gas is quite significant, since it is clear from Fig. 1(a) that the density of samples sintered in Ar are much higher than that of samples sintered in N_2 at the same temperature. In fact, sintering at 1300 °C in Ar is roughly equivalent to sintering in N at 1600 °C. This indicates that the kinetics of the sintering process is strongly dependent on the sintering atmosphere.

A densification curve was made relating sample density to sintering temperature for each of the four sintering environments used for this study and is shown in Fig. 2. From this curve we can see that the N_2 sintered samples are only in the intermediate stage of the sintering process for the temperatures used for this study [16], while the Ar sintered samples are well into the final stages of sintering and appear to have reached thermal stability. Adding hydrogen to the sintering environment seems to have a retarding effect on the sintering and densification of the test samples as seen by the drop in sample density at a given temperature when compared to the samples that were sintered without hydrogen.

The porosity also changes significantly with temperature and sintering gas, as shown in Fig. 1(b) and (c), where it can been seen in that the samples sintered in a 6% hydrogen environment show an increase in open porosity and a small decrease in closed porosity compared to samples sintered without hydrogen.

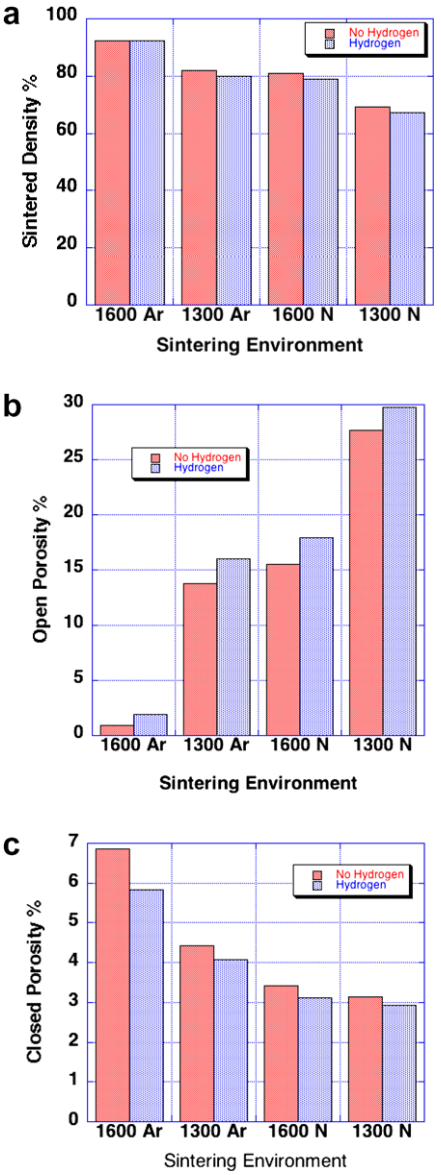

Fig. 1. (a) Sintered density; (b) open and (c) closed porosity as a function of sintering temperature and atmosphere.

3.2. Microstructure

A decrease in closed porosity produced by hydrogen can be noticed in the microstructure of two samples having similar densities, as shown in Figs. 3 and 1(c), where samples sintered with and without hydrogen are compared. Note that the sample sintered in Ar–6% H_2 (Fig. 3(b)) shows a reduction of closed porosity over the sample sintered in pure Ar (Fig. 3(a)). Most of the closed porosity in these samples looks like bubble formations located on

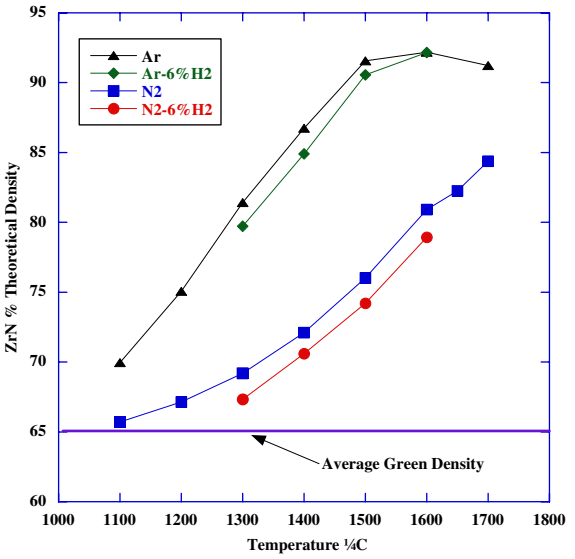

Fig. 2. Densification behavior of ZrN pellets sintered under various atmospheres.

the interior of a grain, particularly at large densities, as can be seen in the SEM pictures of the resulting microstructures shown in Fig. 4. This assumption is made based on the fact that the most energetically favorable shape of a bubble or void is a sphere [17], rather than an irregular or sharp edged shape or a cylinder. So the circular voids in the two-dimensional cross section can be assumed to have been nearly spherical and therefore closed porosity.

Note from Fig. 5(a) that samples sintered in argon at 1600 °C show large pores with clear and porosity coarsening mechanisms associated with grain boundary sweeping. The circular cross section of the pores in the dense samples sintered at 1600 °C in Ar, along with the well-developed grain structure, adds to the suggestion that the microstructure is reaching thermal stability.

The sample sintered in nitrogen at 1300 °C (Fig. 5(b)), shows signs of grain growth by particle coalescence, which is to be expected in the earlier stages of the sintering process. One of the most noticeable microstructural differences of the samples shown in Fig. 4 is the effect that the sintering atmosphere has on grain evolution. There were no observations of fine particles remaining in samples sintered in argon, while all samples sintered in nitrogen exhibited incomplete sintering to some extent. The microstructure of the nitrogen-sintered samples has two distinct regions: dense clusters of small grains and sparse regions of particles that seem to have very little interconnection (Figs. 4(b) and 5(b)). Possible reasons for this could be due to differences in solubility and chemical activity of the two sintering gasses, as well as the population of point defects they produce [17] during sintering. In this sense, the point defects produced by changes in stoichiometry are known to have large effects on transport kinetics in nuclear fuels [2,3,15]. For example, uranium nitride that is nitrogen deficient has been shown to experience more swelling and gas release by accumulation of fission gases on the grain boundaries than nitrogen rich UN [2]. This is probably an effect of enhanced mobility of fission gas due to point defects produced by deviation from stoichiometry, in a manner similar to that observed in oxygen rich UO_2 [15]. The accelerated sintering kinetics under Ar strongly suggests the presence of point defects enhancing mass transport in ZrN.

The lattice parameters measured in samples sintered under Ar and N_2 offer supporting evidence for a difference in defect population between the two sintering conditions. The resulting lattice parameters are shown in Fig. 6. Note from this figure that the lattice parameters are not affected strongly by the presence of hydrogen in the sintering

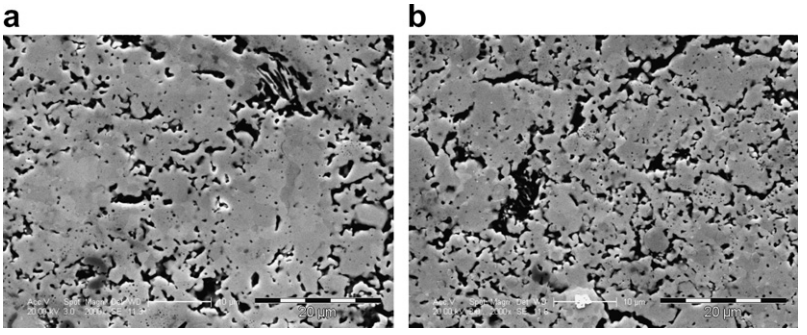

Fig. 3. Typical microstructure of: (a) 1300 °C Ar and (b) 1300 °C Ar–6% H. Scale bar = 20 μm in both figures.

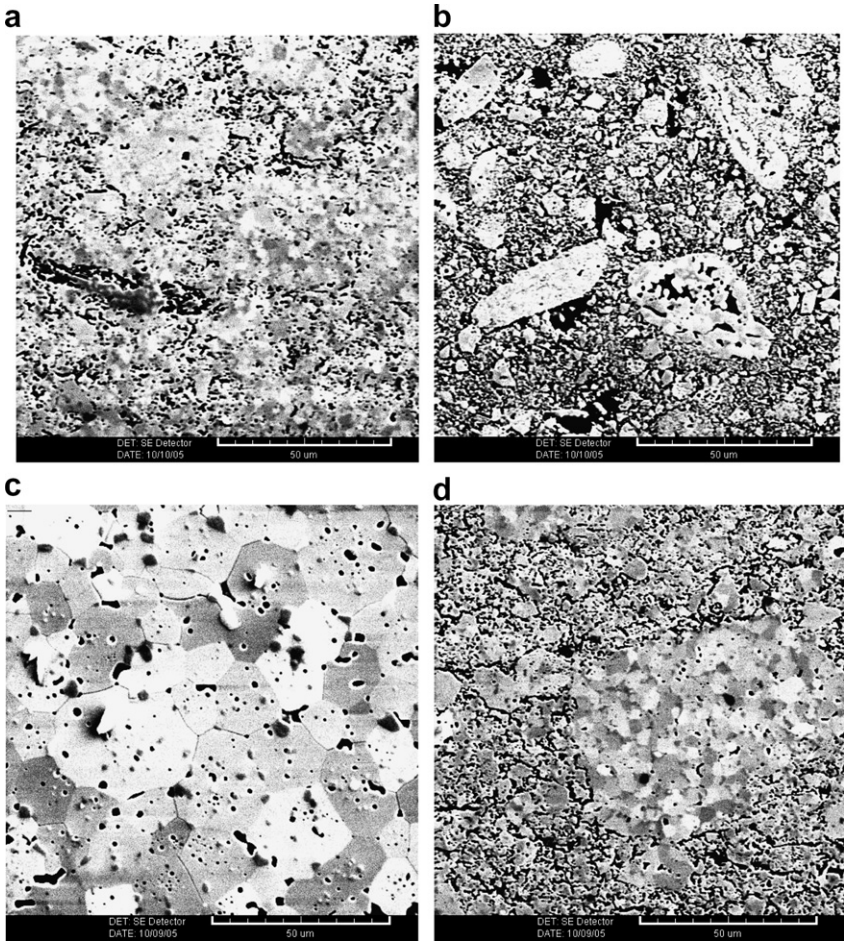

Fig. 4. Typical microstructure of sintered samples. (a) Ar, 1300 °C, (b) N, 1300 °C, (c) Ar, 1600 °C, (d) N, 1600 °C. Scale bar is 50 μm in all images.

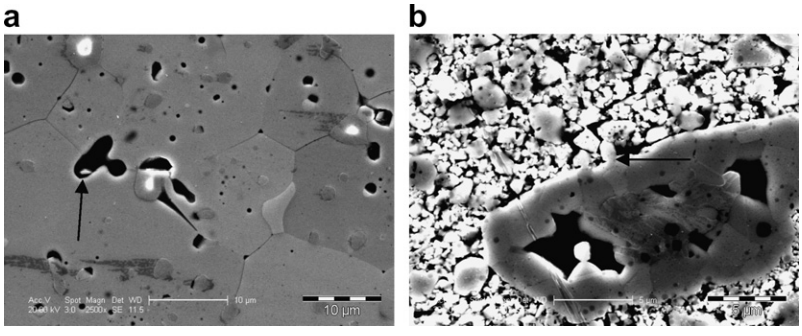

Fig. 5. (a) Pore coalescence (arrow), 1600 °C Argon. Scale bar = 10 μm. (b) Grain growth by particle coalescence (arrow), 1300 °C N. Scale bar = 5 μm.

environment, since the differences are within the error bars shown; however, the differences between Ar and N_2 are significant and larger than the error bars. This result indicates that the sintering atmosphere indeed makes a difference on the material lattice, probably through the generation of point defects. The trend observed, though, is somewhat hard to explain at this time, since the lattice parameter measured for the Ar sample is somewhat closer to the value of a standard database, 4.578 Å

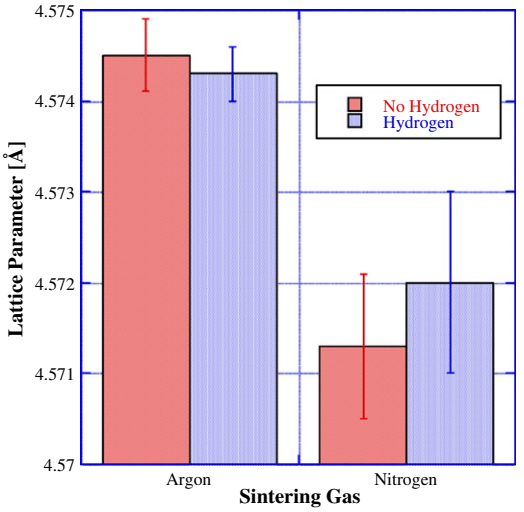

Fig. 6. Lattice parameter in samples sintered at 1600 °C under different atmospheres.

[18], than that of the samples sintered in N_2, which is smaller. The possible reasons for this are being explored. However, the difference between the two cases is clear and measurable, and it points to structural changes induced during sintering, given that the initial powder was the same for both samples.

The difference in microstructure induced by changes in sintering gas were further explored in high density samples, since they present a microstructure that is quite similar to that reported in [3] for UN as a potential material for space fuels. The large grains present in the samples sintered in Ar at high temperature make them suitable to study using orientation imaging microscopy (OIM), as described in the next section.

3.3. Orientation imaging microscopy (OIM)

The orientation data gathered with OIM was used to obtain grain size and grain boundary misorientation distributions for samples sintered in Ar with and without hydrogen, as shown in Fig. 7. The sample size for this study contained ≈1500 grains for each of the two materials. The data were filtered to remove points with more than 10% probability of being incorrect, and the porosity was 'cleaned up' in such a way that only the underlying grain structure was used for the measurement. The differences between the grain size distributions of the samples sintered with and without hydrogen are subtle, but interesting. The average grain size for both of them is about the same at about 20 μm, which is the grain size required for UN in space applications according to [3], pointing to Ar as the best choice for sintering environment in this case, although there is some evidence that vacuum can also be quite effective [2]. Note that the sample sintered in Ar has a sharper maximum, which implies that the grain size is actually more uniform in this sample than in the specimen sintered in Ar–6% H_2, where the distribution is 'blunt' around the maximum value, pointing to a wider distribution of grain sizes. Furthermore, there are two local maxima beyond the average value, which means that there is a tendency for certain grains to grow larger than in the sample sintered in Ar. It should be noted that the variation of the grain size distribution of the Ar–6% H_2 sintered samples could be linked to grain boundary interference by either pores, gas bubbles or solid inclusions based on the tendency for these interactions to create bimodal grain size distributions [16].

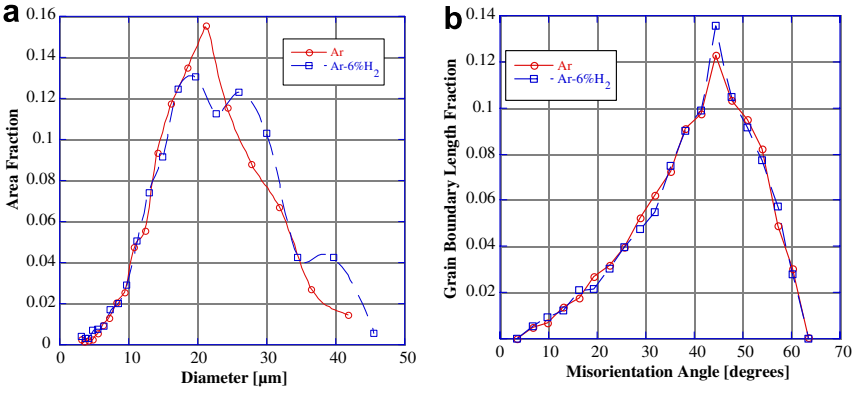

Fig. 7. (a) Grain size distribution and (b) grain boundary misorientation distribution for samples sintered in Ar and Ar–6% H at 1600 °C.

Regarding the distribution of misorientation angles, note that the situation is reversed: the sample sintered in Ar–6% H_2 has a sharper peak than the sample sintered in pure Ar, which means that samples sintered in Ar–6% H_2 have a higher fraction of these boundaries. These peaks are around 45° for both specimens, so that grain boundaries for the two sintering conditions tend to be 'high angle' [19], with a higher fraction of them in samples sintered under the argon–hydrogen atmosphere.

The microstructural differences described above also affected the mechanical response of the samples, which will be discussed below.

3.4. Mechanical response

The Vickers hardness of the samples used in this study is shown in Fig. 8. There is a significant difference between samples sintered in N_2 at 1300 °C and samples sintered in Ar at 1600 °C. In addition, note that the hardness of samples sintered with a 6% addition of hydrogen is lower compared to similar samples sintered without hydrogen. All these trends are likely linked to the differences in microstructure among the samples.

Comparison of the indents made in high density samples sintered with and without hydrogen reveal that indents induced intergranular cracking in both cases, which is not surprising given the presence of a large fraction of high angle boundaries (Fig. 7(b)). However, the region affected by cracking is larger in specimens sintered in Ar–6% H_2, as can be seen in Fig. 9. The fact that the intergranular cracking extends farther in the sample sintered in Ar–6% H_2 suggests that this sample presents relatively weaker grain boundary strength. This agrees with the fact that the average hardness for samples sintered in Ar–6% H_2 is lower and the scatter larger than for samples sintered in pure Ar. The low hardness of samples sintered in N_2, with and without hydrogen, as compared to the hardness of samples sintered in Ar, is simply a result of the differences in density and microstructure. A lower hardness can indeed be expected due to the higher porosity and reduced grain interconnection due to poor sintering in N_2.

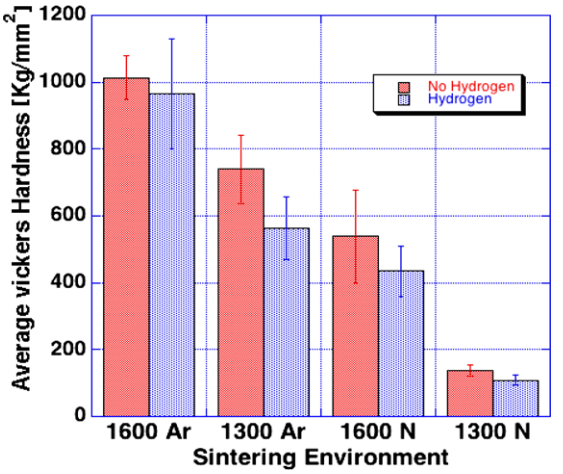

Fig. 8. Vickers hardness as a function of sintering temperature and atmosphere for equivalent load.

The OIM data was also used to establish correlations between the local crystallographic environment around the indents and the fracture behavior. Figs. 10 and 11 show 'typical' indents in samples sintered in Ar and Ar–6% H_2, respectively, along with inverse pole figure (IPF) maps of the grains around these indents. In these IPF maps, the color of each grain correlates to the crystallographic orientation of its normal (coming out of

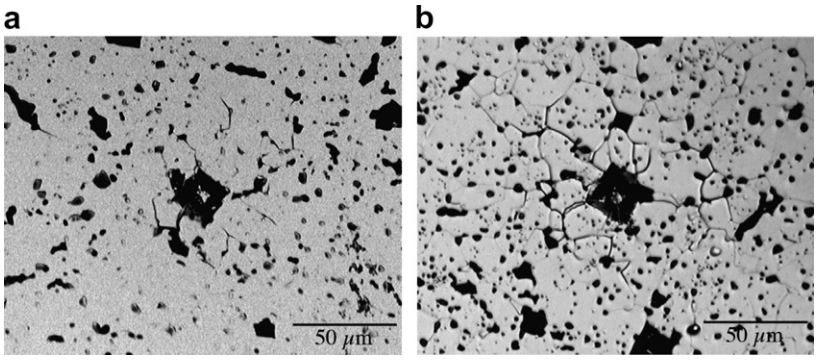

Fig. 9. Optical images of Vickers indents (500 g load) of (a) 1600 °C Ar; (b) 1600 °C Ar–6% H_2 samples. The scale bar in both figures is 50 μm long.

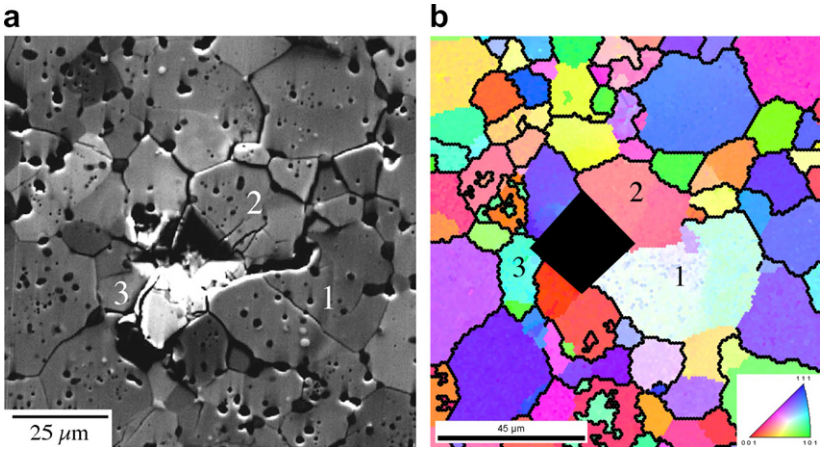

Fig. 10. 'Typical' indent in a sample sintered at 1600 °C in Ar. (a) SEM image and (b) inverse pole figure. The scale bar in (b) is 45 μm long.

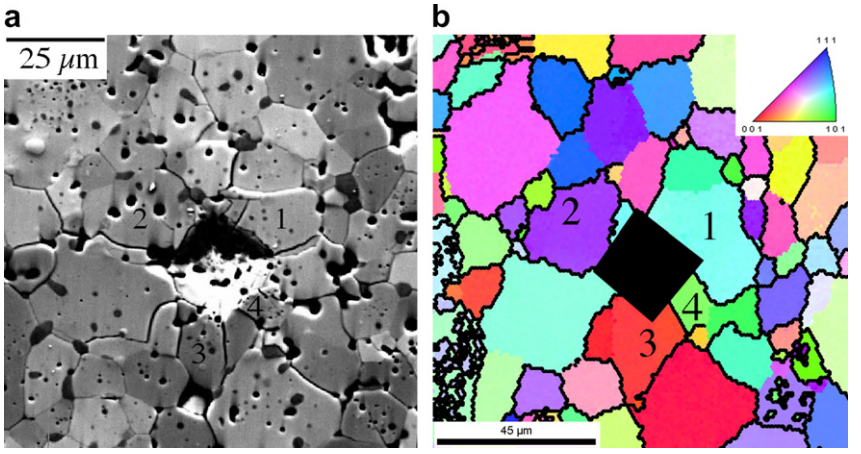

Fig. 11. 'Typical' indent in a sample sintered at 1600 °C in Ar–6% H. (a) SEM image and (b) inverse pole figure. The scale bar in (b) is 45 μm long and thick lines are GB's >30° misorientation angle.

the page) as given by the standard stereographic triangle in the inset of Figs. 10(b) and 11(b). These IPF maps also show the grain boundaries with misorientation angles higher than 30°, as thick black lines. A few grains around the indents are numbered to facilitate their identification. These grains also happen to present transgranular cracks that originate from the corners of the indentation, as would be expected. Note that most of the remaining cracks are intergranular indicating that the grain boundaries, most of which are high angle, are intrinsically weak in ZrN, which is likely to be the case in actinide nitrides as well. This suggests that increasing the fraction of low angle boundaries could lead to improvements in fracture behavior in nitride fuels.

In an effort to identify possible cleavage planes for ZrN the orientation of the traces of the few transgranular cracks observed was measured and the OIM data were used to try to determine if these traces corresponded to low index planes. The angles were measured with respect to the horizontal, and positive values correspond to a counterclockwise rotation. The results are shown in Table 1.

The following low index plane families were used for the match: {001}, {110}, {111}, {012}, {112}, and {113}, chosen because they have low indices [20]. Only those planes with traces that matched the experimental values within 5° are shown. Plane families with more than one value of the calculated trace angle had two or more 'family members' with trace angles within the given tolerance. Results

Table 1
Traces of transgranular cracks around Vickers indents in samples sintered at 1600 °C in Ar or Ar–H

Sample	Grain	Trace angle Θo (observed) (°)	Possible planes	Trace angles Θc (calculated) (°)	$\lvert\Delta\Theta\rvert$ (°)
Ar/1600 °C	1	−34.2	{012}	−38.2	4.0
			{113}	−29.0	5.2
Ar/1600 °C	2	57.9	{112}	59.0	1.1
				60.4	2.5
Ar/1600 °C	2	39.3	{113}	36.7	2.6
			{001}	43.0	3.7
Ar/1600 °C	3	10.0	{112}	9.9	0.1
				11.0	1.0
Ar–H_2/1600 °C	1	20.1	{112}	23.5	3.4
			{012}	16.2	3.9
				15.7	4.4
Ar–H_2/1600 °C	1	60.5	{001}	59.0	1.5
			{113}	61.4	0.9
			{112}	62.5	2.0
			{111}	65.0	4.5
Ar–H_2/1600 °C	2	−5.2	{111}	−5.0	0.2
Ar–H_2/1600 °C	3	93.9	{112}	93.7	0.2
				88.7	5.2
			{012}	91.2	2.7
			{113}	97.6	3.7
Ar–H_2/1600 °C	4	−38.4	{113}	−38.6	0.2
			{112}	−36.5	1.9
			{001}	−43.0	4.6

indicate that the crystallographic plane that matched the observed cracks more times was {112}, followed by {113}. Further measurements using the same methodology are being performed to collect more statistics, which will allow evaluating the likelihood of fracture along low index planes. Similar measurements will also be carried out in actual fuels, in an effort to establish clear relationships between local crystallography, microstructure and mechanical properties in nuclear fuels.

3.5. Discussion

For the application of sintered ZrN as an inert matrix for transmutation fuels, an open porosity increase will aid in the dissipation of the large amount of helium produced by americium during transmutation. However, increasing open porosity by adding hydrogen to the sintering environment could have adverse effects on the mechanical integrity and longevity of the fuel pellet.

In this study we have noticed that by adding hydrogen to the sintering environment we have noticed list of side effects:

1. A retardation of sample densification for given temperature.
2. A decrease in closed porosity.
3. A small change in the grain misorientation distributions.
4. A subtle but interesting development of a bimodal grain size distribution indicative of pore, bubble or inclusions interacting with the grain boundaries during grain growth.
5. A consistent decrease in hardness.
6. An increase in intergranular cracking.
7. Weaker grain boundaries.

In addition to the above side effects, TEM was performed on a HIPed sample of ZrN in order to try and evaluate the effects hydrogen has on the grain boundary. Fig. 12 is a TEM of a HIPed sample that was heat treated in a N_2–6% H_2 environment at 1400 °C for 36 h. Note that the diamond shaped voids was not found in the part of the sample that was not heat-treated (TEM not shown). While we are not positive what the formations are at this time, several possibilities exist that involve hydrogen, such as a hydride formation, a pore or a hydrogen bubble that has collapsed allowing the energy of the surrounding crystal structure to dictate the shape of the resulting void rather than the typical spherical shape cause by sufficient internal pressure.

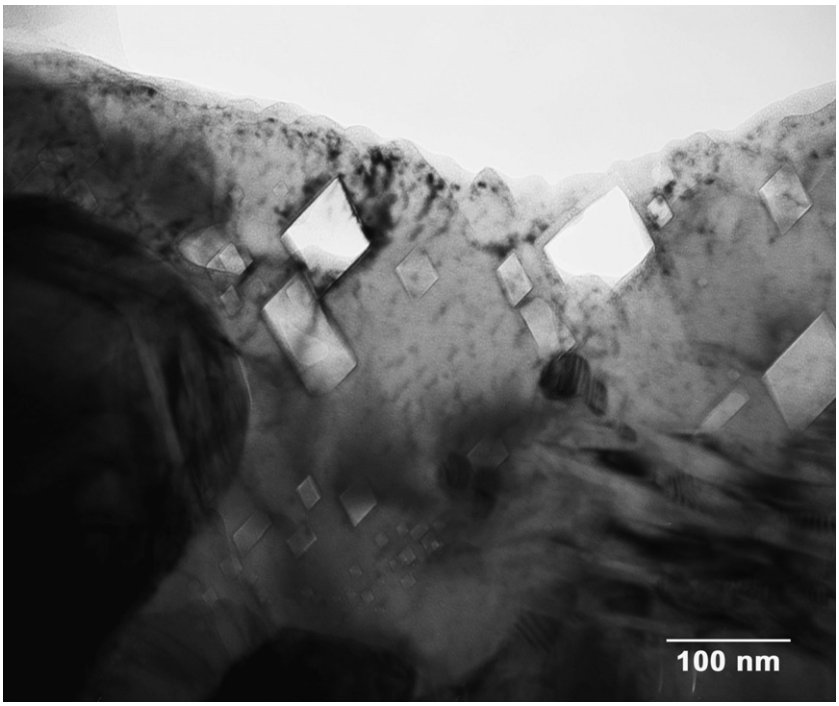

Fig. 12. TEM image of formations found in HIPed ZrN sample after 36 h heat-treatment in N_2–6% H_2 environment at 1400 °C.

Hydrogen is likely to effect the sample's grain growth kinetics due to the negative effect it has on heterogeneous nucleation, by far the most common form of grain nucleation mechanism observed during sintering [17]. Heterogeneous nucleation is induced when surfaces, grain boundaries, second-phase particles and other structural discontinuities serve as favorable nucleation sites. The driving force of such nucleation is the reduction of the surface energy of individual particles. As the material is heated, the surface tension of the particles is reduced, which allows the materials to deform and flow to a more energetically favorable position.

Grain growth relies on available feed material and sufficient temperature. The kinetics of this process indicates that at sufficient temperature grain growth will occur when atoms move from the convex to the concave side of a grain boundary. As the volume of one grain increases, the grain boundary area is increased in order to preserve static equilibrium. As the grain boundary moves it must pull impurities or bubbles that are attracted to the grain boundary [17]. If hydrogen migrates to the surface, or near the surface, of grains during sintering, or hydrides are forming and it is more energetically favorable to have them on the boundaries, then it will take more energy for two adjacent particles to neck and coalesce if they must displace the inclusions located on the surface. It is possible to now offer an possible explanation for the side effects listed previously.

Gas filled pores and bubbles that are moved by grain boundaries during grain growth can collide and coalesce. However, in samples sintered under hydrogen the motion of closed pores could be reduced by a decrease in grain boundary mobility, due to the increased movement resistance caused by, for example, possible hydride formations and/or hydrogen bubbles on or near grain boundaries. Reduced grain boundary mobility would, in turn, result in a reduction of closed pore formation and a higher open porosity (adjacent particles that have failed to coalesce).

The results of the grain boundary and misorientation angle distributions tend to support the idea that hydrogen could have affected the sintering process through the presence of either hydrogen or hydrides at the grain boundaries. In this sense, high angle boundaries tend to be sites for segregation and precipitation, since they typically have more energy and free volume [19]. The presence of hydrogen (or hydrides) in particular boundaries would tend to 'pin' them, keeping them from moving or changing character, whereas boundaries without these

impurities could move more freely. This can be used to explain the sharper peak of the misorientation angle in the Ar–6% H_2 sample, and the bimodal grain size distribution, since some grains would be able to grow larger than others due to differences in grain boundary mobility.

4. Conclusions

Studies of microstructure and mechanical properties of ZrN sintered under different conditions lead to the following conclusions:

- Using an Ar atmosphere leads to faster sintering and increased grain growth kinetics than those obtained using nitrogen. The microstructures obtained in the Ar atmosphere are similar to those specified for UN in space applications such as nuclear–thermal propulsion and seem to be thermally stable, given the presence of equiaxed grains and pores.
- Lattice parameter measurements indicate that there are structural differences between samples sintered in different atmospheres for a given temperature. It is likely that point defects produced by changes in stoichiometry are playing a role on the kinetics of mass transport during sintering.
- The presence of hydrogen in the sintering environment does not affect the final density significantly; however, it leads to a higher fraction of open porosity, a wider grain size distribution and a tendency to produce a larger fraction of high angle boundaries. This could be due to interactions between either hydrogen or hydrides with the grain boundaries.
- Vickers hardness measurements indicate that the presence of hydrogen leads to lower average values of hardness, which correlate with a larger zone of intergranular cracking around indents. This, in turn, suggests that hydrogen produced grain boundary embrittlement in ZrN.
- High angle grain boundaries are generally weak in ZrN, suggesting that methodologies to increase the fraction of low angle boundaries may be useful to increase the reliability of nitride fuels.
- TEM of HIPed ZrN samples show formations near the grain boundary that are produced with heat-treated in a N_2–6% H_2 environment.
- Local crystallographic orientation data can be used to understand deformation and fracture behavior in nitride fuels and ceramic materials.

Acknowledgement

This project was partially funded by the Department of Energy under the Advanced Fuel Cycle Initiative (AFCI) under Contract #DE-FC07-05ID14654 at Arizona State University, in addition to resources provided by LANL.

References

[1] AFCI Program Plan, 2005.
[2] B. Ma, Nuclear Reactor Materials and Applications, Van Nostrand Reinhold Publishing, New York, 1983.
[3] R.B. Matthews, K.M. Chidester, C.W. Hoth, R.E. Mason, R.L. Petty, J. Nucl. Mater. 151 (1988) 334.
[4] B.N. Kiforenko, I.Y. Vasil'ev, Acta Astronaut. 54 (2002) 61.
[5] K. Minato, M. Akabori, M. Takano, Y. Arai, K. Nakajima, A. Itoh, T. Ogawa, J. Nucl. Mater. 320 (2003) 18.
[6] L. Koch, in: Handbook on the Physics and Chemistry of the Actinides, vol. 457, 1986.
[7] Y. Arai, K. Nakajima, J. Nucl. Mater. 281 (2000) 244.
[8] M. Burghartz, G. Ledergerber, H. Hein, R.R.vd. Laan, R.J.M. Konings, J. Nucl. Mater. 288 (2001) 233.
[9] R.J.M. Konings, K. Bakker, J.G. Boshoven, H. Hein, M.E. Huntelaar, R.R.vd. Laan, J. Nucl. Mater. 274 (1999) 84.
[10] M. Streit, F. Ingold, M. Pouchon, L.J. Gauckler, J.P. Ottaviani, J. Nucl. Mater. 319 (2003) 51.
[11] C.T. Walker, G. Nicolaou, J. Nucl. Mater. 218 (1995) 129.
[12] J.C. Spirlet, W. Muller, J. Less-Common Met. 31 (1973) 35.
[13] T. Ogawa, T. Ohmichi, A. Maeda, Y. Arai, Y. Suzuki, J. Alloy. Comp. 224 (1995) 55.
[14] V. Sobolev, S. Lemehov, N. Messaoudi, P.V. Uffelen, H.A. Abderrahim, J. Nucl. Mater. 319 (2003) 131.
[15] D.R. Olander, Fundamental Aspects of Nuclear Fuel Elements, Technical Information Center, Office of Public Affairs, Energy Research and Development Administration, 1976.
[16] J.S. Reed, Principles of Ceramics Processing, Wiley Inter-Science, New York, 1995.
[17] W.D. Kingery, Introduction to Ceramics, John Wiley, New York, 1976.
[18] Data IICfD, PDF# 00-035-0753 (ZrN), 2006.
[19] A.P. Sutton, R.W. Ballufi, Interfaces in Crystalline Materials, Oxford University, New York, 1995.
[20] G.E. Dieter, Mechanical Metallurgy, New York, 1986.